analytical chemistry

Letter

Cite This: *Anal. Chem.* 2019, 91, 4301−4306

pubs.acs.org/ac

BODIPY-Based Fluorescent Probe for Dual-Channel Detection of Nitric Oxide and Glutathione: Visualization of Cross-Talk in Living Cells

Xiao-Xiao Chen, Li-Ya Niu,* Na Shao, and Qing-Zheng Yang*

Key Laboratory of Radiopharmaceuticals, Ministry of Education, College of Chemistry, Beijing Normal University, Beijing 100875, P. R. China

Supporting Information

ABSTRACT: Nitric oxide (NO) and glutathione (GSH) have interplaying roles in oxidant-antioxidant balance. In this work, we developed the first example of a single fluorescent probe that displayed a turn-on fluorescence response toward NO and GSH from dual emission channels. The probe was synthesized by introducing 4-amino-3-(methylamino)-phenol to a BODIPY scaffold. Specifically, the NO-mediated transformation of diamine into a triazole triggered the fluorescence in the green channel, and the GSH-induced S_NAr substitution reaction led to the red-shifted emission in the red channel. The probe was successfully applied to detect the exogenous and endogenous NO and GSH in macrophage cells. More importantly, the probe revealed that NO induced by interferon-γ (IFN-γ), lipopolysaccharide (LPS), and L-arginine (L-Arg) could also elicit the augmentation of intracellular GSH. We anticipate the probe would hold great potential for investigating the redox balance in biological processes.

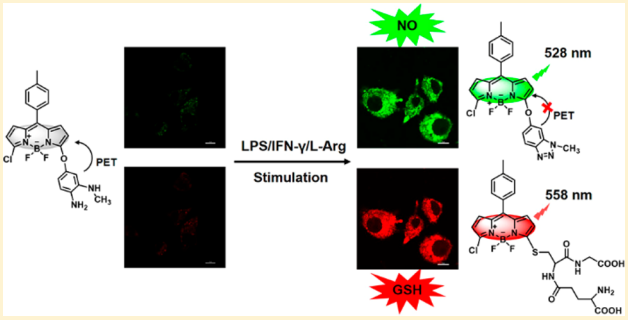

Reactive nitrogen species (RNS) and reactive sulfur species (RSS) play interrelated roles in the redox homeostasis of biological systems.[1] Nitric oxide (NO), acting as a ubiquitous signaling molecule, is a representative RNS and plays a key role in multiple biological processes such as regulating relaxation, blood pressure modulation, and peristalsis.[2] Moreover, low doses of NO have a protective and proliferative influence on cells, while high doses lead to nitrosative stress that is related to autoimmune and inflammatory diseases including ischemia stroke and rheumatoid arthritis.[3] GSH, one of the essential RSS, is the most abundant small molecule biological thiol. It is an effective endogenous antioxidant that eliminates toxins and free radicals by conjugating with them. GSH can scavenge NO to form nitrosoglutathione (GSNO), which prevents cells from deleterious effects of nitrosative stress.[4] To understand the complicated inter-relationship between them, the simultaneous detection of NO and GSH is highly valuable.

Fluorescent probes have served as an attractive tool to sensing and imaging biomolecules owing to the high sensitivity and selectivity coupled with nondestructive imaging properties and ease of use.[5−8] Traditionally, most fluorescent probes require a highly selective response toward a single analyte. A variety of fluorescent probes have been utilized for NO or GSH detection separately. NO imaging was achieved under physiological conditions through the specific reactions of NO with an *o*-phenylenediamino (OPD) moiety,[9−11] metal−ligand complexes,[12−15] N-nitrosation of aromatic secondary amines,[16−18] and others.[19,20] Among them, the OPD moiety is the most versatile NO reaction site and is utilized in many fluorescent probes for NO detection. In terms of sensing GSH, by using the strong nucleophilicity of GSH, many fluorescent probes have been developed by Michael addition,[21,22] cleavage of the disulfide,[23,24] sulfonamide,[25] and so on.[26−29] Our group has developed highly sensitive and selective BODIPY-based ratiometric fluorescence sensors for discrimination of GSH over Hcy/Cys.[30] Suzuki and co-workers have pointed out that using two or more individual fluorescent probes for dual or multianalyte detection results in many defects, including potential cross-talk among the various fluorescent probes, the complicated situation on account of the different localization and photobleaching rates of individual probes.[31] To clarify the relationship and interplay between the analytes in complicated physiological processes, the development of a single fluorescent probe that can selectively distinguish them from different emission channels is highly desirable but still a challenge. To the best of our knowledge, there is no example of a single fluorescent molecule that can respond to NO and GSH simultaneously with distinct fluorescence signals. Herein, we report a fluorescent probe for simultaneous detection of NO and GSH from different emission channels (Scheme 1). The probe was composed of a BODIPY moiety as the fluorescence reporter and 4-amino-3-(methylamino)-phenol moiety as the

Received: January 10, 2019
Accepted: March 4, 2019
Published: March 4, 2019

DOI: 10.1021/acs.analchem.9b00169
Anal. Chem. 2019, 91, 4301−4306

Scheme 1. Proposed Mechanism for the Reactions of Probe 1 with NO/GSH

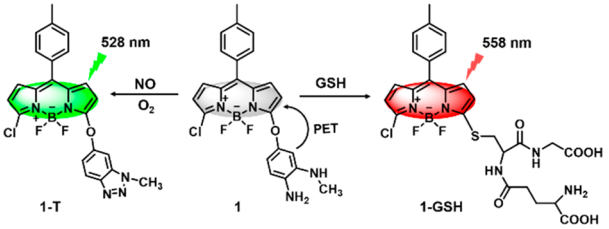

NO- and GSH-responsive fluorescence modulator. Under aerobic conditions, the 4-amino-3-(methylamino)-phenol unit controlled the fluorescence off-on switching in the green channel based on the change of the electron-donating ability upon selective NO-mediated transformation of the diamine into a triazole.[32] Additionally, the 4-amino-3-(methylamino)-phenol moiety was expected to be replaced by GSH through an S_NAr substitution reaction, leading to the red-shifted emission in the red channel.[33,34] The probe was used to detect the exogenous and endogenous NO and GSH in macrophage cells, revealing the cross-talking relationship in keeping the oxidant-antioxidant balance of biological system.

Initially, we designed compounds **1**−**3** for the detection of NO (Scheme 2). The *o*-phenylenediamino (OPD) moiety with

Scheme 2. Structures of 1−3

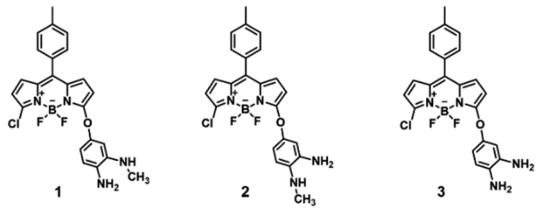

electron-donating ability is a common NO specific reaction group, which quenches the emission of the probe through a photoinduced electron transfer (PET) mechanism.[32] In the presence of NO, the diamine transforms into a triazole with electron-withdrawing ability, thus the PET process is blocked and the fluorescence is turned on. On the other hand, according to our previous work,[33,34] phenol derivatives attaching to the BODIPY core were supposed to be replaced by GSH through an S_NAr substitution reaction and resulted in red-shifted emission. As studied in our previous work,[30] the push−pull electronic capability of the substituents at the 3-position of BODIPY affected the reactivity of nucleophilic aromatic substitution. Thus, the electron-withdrawing chlorine at the 3-position would enable the fast response of the probe toward GSH. Therefore, we intended to introduce a 3,4-amino (or methylamino) phenol to the chlorinated BODIPY to obtain a fluorescent probe that can be responsive to NO and GSH with different fluorescence signals. Bearing the above anticipations in mind, compounds **1**−**3** were synthesized from 3,5-dichlorinated BODIPY as a precursor. First, 4-nitro-3-(methylamino)-phenol, 4-(methylamino)-3-nitrophenol, and 4-amino-3-nitrophenol were attached to the 3-position of dichlorinated BODIPY through an S_NAr substitution reaction, and then the nitro groups were reduced to amino groups using $SnCl_2{\cdot}2H_2O$, 98% HCl under N_2 to generate **1**−**3**, respectively. Compounds **1**−**3** were well characterized by ^1H NMR and ^{13}C NMR spectroscopy and high-resolution mass spectrometry (HRMS).

Subsequently, we performed the fluorescent responses of **1**−**3** toward NO. Probes **1**−**3** have weak or almost no fluorescence due to the PET process. When **1**−**3** is incubated with DEA·NONOate (a commercially available NO donor with a half time of 16 min), the fluorescence intensity at 528 nm increased to different extents (I/I_0 = 230-, 80-, and 4-fold for **1**−**3**, respectively) (Figure 1a−c) when excited at the

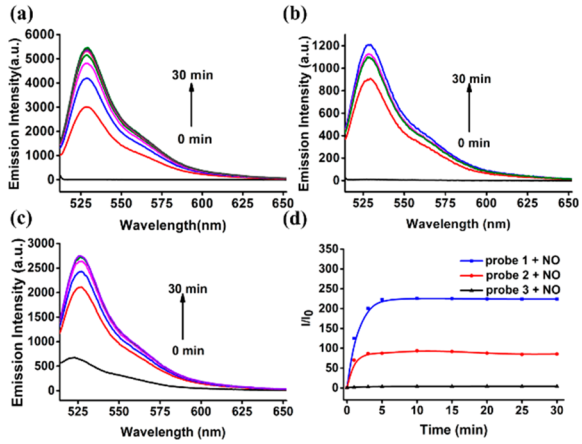

Figure 1. (a−c) Time-dependent fluorescence spectra of **1**−**3** (10 μM) upon addition of DEA·NONOate (200 μM). (d) Time-dependent fluorescence intensity changes of probe **1**−**3** toward DEA·NONOate (200 μM). Each spectrum was recorded in PBS buffer (10 mM, pH 7.4, containing 30% CH_3CN) after 30 min addition at 37 °C. λ_{ex} = 505 nm, λ_{em} = 528 nm.

absorption maximum of the product at 505 nm (Figure S1a). In keeping with the above-mentioned mechanism, the formation of triazole, which was confirmed by ^1H NMR spectroscopy and HRMS experiments, suppressed the PET process and led to fluorescence recover (Figures S17 and S29). Probe **3** showed only 4-fold fluorescence enhancement, while **1** displayed the most significant fluorescence enhancement of 230-fold.

Further theoretical calculations confirmed that the fluorescence quenching of compounds **1**−**3** should be caused by the PET mechanism. The TD-DFT/PCM results show that the S_1 state is a clear excited charge transfer state, which is mainly caused by electronic transition from the highest occupied molecular orbital (HOMO) to the lowest unoccupied molecular orbital (LUMO) (Figure 2). These two MOs

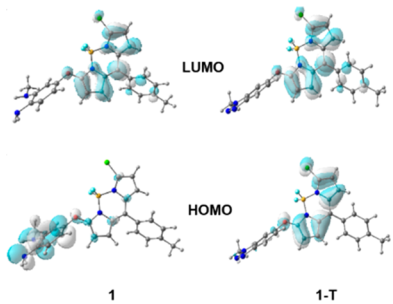

Figure 2. HOMO and LUMO of compound **1** and its triazole product **1-T** calculated at the TD-DFT/PCM level (see the Supporting Information for those related to **2**, **3**, **2-T**, and **3-T**).

DOI: 10.1021/acs.analchem.9b00169
Anal. Chem. 2019, 91, 4301−4306

are primarily located on both BODIPY and phenol moieties, respectively, so there is nearly no overlap between HOMO and LUMO leading to a small oscillator strength of ~0.1 at the TD-DFT/PCM level. These results indicate that the S_1 state is a dark state and could be nonfluorescent.[35] On the contrary, for **1-T**, **2-T**, and **3-T**, the S_1 state is a clear locally excited singlet state, which as well corresponds to an electron moving from HOMO to LUMO (Figure 2 and Figure S9). However, in this situation, these two MOs are all essentially located on BODIPY fragment thus leading to a large overlap. As a result, the S_1 state becomes highly fluorescent due to its large oscillator strength of ~0.8 at the same computational level. The above theoretical results are also seconded by our following experiments.

We speculated that the higher sensitivity of **1** and **2** compared to **3** was attributed to two aspects. First, the methylamino groups in **1** and **2** showed a stronger electron-donating ability than **3**, thus the emission of **1** and **2** was quenched to a greater extent and resulted in less fluorescence relative to **3**. Second, the deprotonation of the benzotriazole **3-T** under physiological conditions would form an electron-rich triazolate **3-R**, which still suffered from fluorescent quenching through a weak PET process (Scheme 3). The PET process

Scheme 3. Deprotonation of 3-T

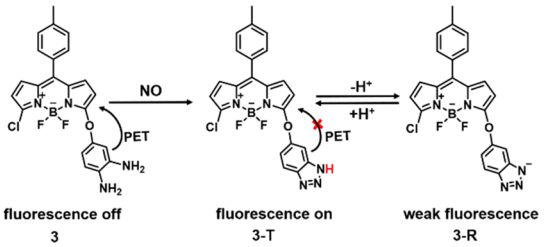

was also supported by theoretical calculations (Figure S9). Conversely, triazole products **1-T** and **2-T** (Scheme S1) without NH proton would not go through PET-induced fluorescence quenching under physiological conditions, thereby showing brighter fluorescence than **3-T**.[36] (Figure 1d).

In order to further support the above speculations, we also investigated the fluorescent property of **1** and **3** treated with DEA·NONOate at different pH values. As shown in Figure S2a,c, **1** showed almost no fluorescence changes in the presence of DEA·NONOate at physiological pH ranging from 4 to 9. By comparison, compound **3**, after the addition of DEA·NONOate, displayed significant fluorescence enhancement under acidic conditions (pH 4−6) but a less distinct increase in the region of 7−9, which further confirmed that the benzotriazole was deprotonated to form the electro-rich triazolate under high pH values, resulting in fluorescent quenching via the PET process. These results demonstrated that probe **1** is more advantageous for the detection of NO and could be conducted in a wide range of pH values, exhibiting a higher sensitivity at physiological conditions. Thus, probe **1** was chosen as a candidate for the detection of NO.

Consequently, we tested the changes in the emission spectra of **1** with different concentrations of DEA·NONOate. With incremental amounts of DEA·NONOate, the emission intensity at 528 nm was notably enhanced. There was a great linearity (R^2 = 0.996) between the fluorescent intensity and the concentration of DEA·NONOate ranging from 0 to 50 μM (Figure 3a,b). The detection limit for DEA·NONOate was

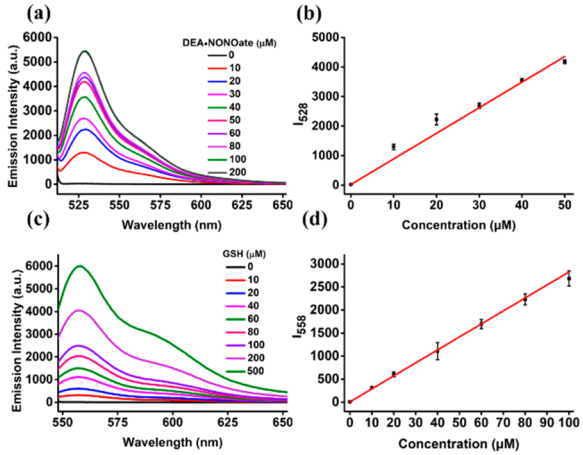

Figure 3. (a) Fluorescence spectra of probe **1** (10 μM) treated with DEA·NONOate (0−200 μM) in PBS buffer (10 mM, pH 7.4, containing 30% CH_3CN). (b) Corresponding linear relationship between the fluorescent intensity and DEA·NONOate concentration. Spectra were recorded after incubation with different concentrations of DEA·NONOate for 30 min. λ_{ex} = 505 nm, λ_{em} = 528 nm. (c) Fluorescence spectra of probe **1** (10 μM) treated with GSH (0−500 μM) in PBS buffer (10 mM, pH 7.4, containing 30% CH_3CN). (d) Corresponding linear relationship between the fluorescent intensity and GSH concentration. Spectra were recorded after incubation with different concentrations of GSH for 30 min. λ_{ex} = 538 nm, λ_{em} = 558 nm.

determined to be 3.1 × 10^{-8} M (S/N = 3). Next, we measured the fluorescence response of **1** toward GSH. Upon treatment with GSH, **1** exhibited an 1800-fold increased emission at 558 nm when excited at the absorption maximum of the product at 538 nm (Figures S1a and S3a). To study the reaction mechanism, control reactions of **1** with methyl mercaptoacetate as a model compound generated compound **BC-S**, characterized by ^{1}H NMR, whose fluorescent spectra matched well with those of **1-GSH**(Figure S1b). Moreover, the formation of **1-GSH** was confirmed by HRMS experiments (Figure S31). We proposed that the 4-amino-3-(methylamino)-phenol group of **1** is replaced by the thiol group of GSH to give compound **1-GSH**. Also, we examined the performance of **1** to various concentrations of GSH. The fluorescence intensity at 558 nm increased linearly (R^2 = 0.997) as the concentration of GSH was increased up to 100 μM (Figure 3c,d). The corresponding detection limit was determined to be 5.6 × 10^{-8} M (S/N = 3).

We further studied the fluorescence properties of probe **1** toward NO and GSH when they coexisted in mixtures of PBS buffer (10 mM, pH 7.4, containing 30% CH_3CN) at 37 °C. Interestingly, upon addition of DEA·NONOate and GSH simultaneously (Figure 4), the peak at 528 nm increased rapidly at the beginning, and then the fluorescence peak at 558 nm emerged and increased gradually when the emission at 528 nm reached a plateau within 30 min, probably because the reaction rate of **1** with NO (k_{NO} = 0.346 min^{-1}) was much faster than that of GSH (k_{GSH} = 0.015 min^{-1}) (Figure S4). The above results demonstrated that this probe can detect coexistent NO and GSH from dual channels.

To examine the selectivity, we studied the fluorescence spectra of **1** toward different biologically relevant species, which were classified as reactive oxygen/nitrogen species (ROS/RNS, NO_3^-, NO_2^-, $^1O_2$, $^{\bullet}OH$, H_2O_2, O_2^-, and $ONOO^-$), reactive sulfur species (SO_4^{2-}, SO_3^{2-}, $S_2O_5^{2-}$,

DOI: 10.1021/acs.analchem.9b00169
Anal. Chem. 2019, 91, 4301−4306

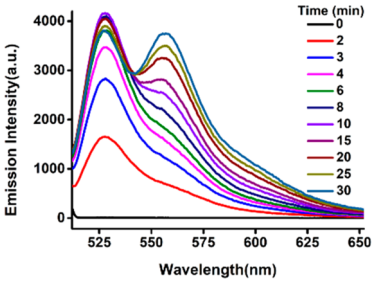

Figure 4. Time-dependent fluorescence spectra of probe **1** (10 μM) upon addition of DEA·NONOate (200 μM) in the presence of GSH (200 μM). λ_{ex} = 505 nm, λ_{em} = 528 and 558 nm.

HSO_4^-, HSO_3^-, HS^-), various amino acids (His, Iso, Leu, Lys, Met, and Ser), and active biothiols (Cys, Hcy). As shown in the Figure 5a, upon excitation at 505 nm, DEA·NONOate

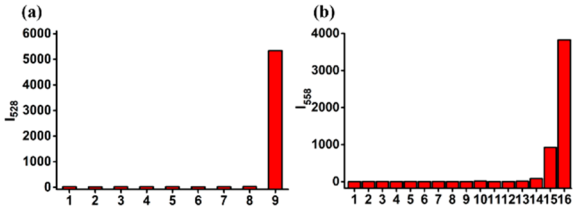

Figure 5. (a) Fluorescence intensities of probe **1** (10 μM) upon addition of 20 equiv of various species after 30 min. (1) Blank, (2) NO_3^-, (3) NO_2^-, (4) $^1O_2$, (5) $^{\bullet}OH$, (6) H_2O_2, (7) $O_2^{\bullet-}$, (8) $ONOO^-$, (9) DEA·NONOate λ_{ex} = 505 nm, λ_{em} = 528 nm. (b) Fluorescence intensities of probe **1** (10 μM) upon addition of 20 equiv of various species after 30 min: (1) blank, (2) His, (3) Iso, (4) Leu, (5) Lys, (6) Met, (7) Ser, (8) SO_4^{2-}, (9) SO_3^{2-}, (10) $S_2O_5^{2-}$, (11) HSO_4^-, (12) HSO_3^-, (13) HS^-, (14) Cys, (15) Hcy, and (16) GSH. λ_{ex} = 538 nm, λ_{em} = 558 nm.

induced a significant fluorescence enhancement of **1** at 528 nm, while a negligible fluorescence increase was observed in the presence of other species. On the other hand, upon excitation at 538 nm, only GSH caused a significant increase in fluorescence at 558 nm. Although Hcy also caused a slight fluorescence enhancement, the concentration of Hcy in the serum is in the range of 9−13 μM, which is much lower than that of GSH.[37] As shown in Figure S3b, when the concentration of Hcy was 20 μM, almost no fluorescence variations at 558 nm were observed, indicating that Hcy would not cause interference for the detection of GSH. Taken together, these results demonstrated that probe **1** was highly selective for NO and GSH at different emission channels.

Encouraged by the desirable results in aqueous solution, we further investigated the capability of probe **1** to sense NO and GSH in living cells using confocal fluorescence microscopy (green channel collected at 510−530 nm, red channel collected at 555−590 nm). After being pretreated with *N*-ethylmaleimide (NEM, a thiol scavenger), RAW 264.7 cells stained by **1** showed almost no fluorescence in both green and red channels (Figure 6a1−c1). Then, the RAW 264.7 cells continued to be loaded with DEA·NONOate after treatment with NEM, resulting in an obvious enhancement in the green channel (Figure 6a2−c2). The fluorescent ratio of the green/red channels was >1 (Figure S5a). When RAW 264.7 cells were only incubated with **1** for 10 min, they displayed strong fluorescence in the red channel (Figure 6a3−c3) with a green/red ratio <1 (Figure S5b), indicating that **1** is responsive to

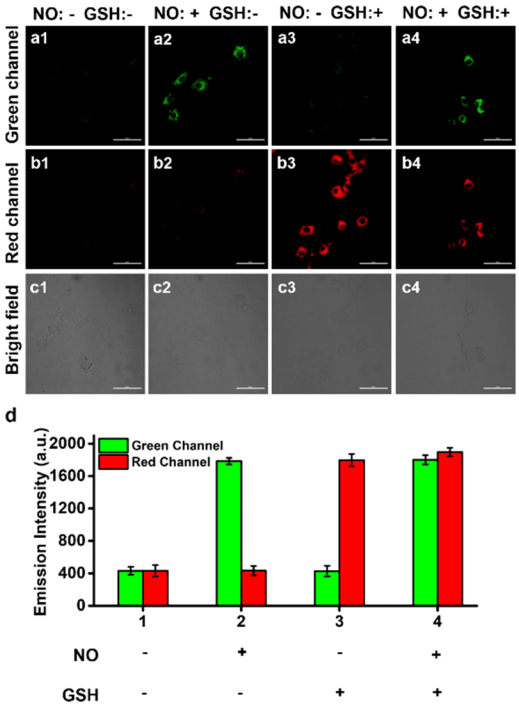

Figure 6. (a1−c1) Confocal fluorescence and bright-field images of RAW 264.7 cells stained by NEM (1 mM, 15 min) and then **1** (2 μM, 10 min). (a2-c2) Confocal fluorescence and bright-field images of RAW 264.7 cells stained by NEM (1 mM, 15 min), DEA·NONOate (200 μM, 10 min), and then **1** (2 μM, 10 min). (a3−c3) Confocal fluorescence and bright-field images of RAW 264.7 cells stained with **1** (2 μM, 10 min). (a4−c4) Confocal fluorescence and bright-field images of RAW 264.7 cells stained by DEA·NONOate (200 μM, 10 min) and then **1** (2 μM, 10 min). (d) Mean fluorescence intensity of green and red channels. Emission was collected at 510−530 nm for green channel (excited at 487 nm) and at 555−590 nm for red channel (excited at 487 nm). Scale bar: 50 μm.

intracellular GSH. Moreover, when the cells were pretreated with DEA·NONOate for 10 min and then further incubated with **1** for 10 min; strong fluorescence in both green and red channels was observed (Figure 6a4−c4), and the ratio of the emission from green and red was ∼1 (Figure S5c), confirming that **1** is able to detect NO and GSH simultaneously in RAW 264.7 cells. The results indicated **1** was capable of imaging NO and GSH from different emission channels in living cells. The low cytotoxicity of **1** was also proven by CCK8 assay (Figure S6).

In addition, we investigated the sensing properties of probe **1** of the endogenous NO in RAW 264.7 cells (green channel collected at 500−550 nm, red channel collected at 550−600 nm). There was weak fluorescence in both green and red channels when RAW 264.7 cells were stained by **1** alone (Figure 7a−c). It has been reported that interferon-γ (IFN-γ), lipopolysaccharide (LPS), and L-arginine (L-Arg) can induce expression of nitric oxide synthase (iNOS), which results in micromolar quantities of NO production.[38,39] To our surprise, RAW 264.7 cells stimulated with IFN-γ/LPS/L-Arg and **1** showed obvious fluorescence enhancement in both green and red channels, suggesting both NO and GSH were elevated (Figure 7d−f). To further confirm this phenomenon, we did the control experiments with compound **B-SH** which only reacted with GSH but not NO (Figure S7). RAW 264.7 cells incubated with compound **B-SH** exhibit no fluorescence in the

DOI: 10.1021/acs.analchem.9b00169
Anal. Chem. 2019, 91, 4301−4306

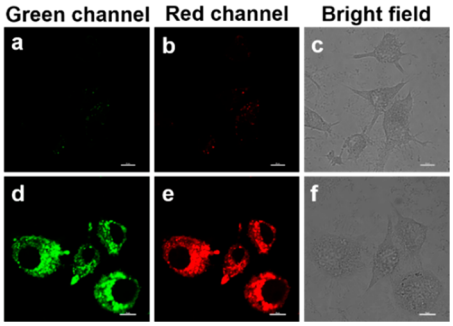

Figure 7. Endogenous NO and GSH detection in RAW 264.7 cells stained by probe **1** (2 μM, 10 min) without (a–c) and with (d–f) the stimulation of 20 μg/mL LPS, 50 μg/mL L-Arg, 0.01 μg/mL IFN-γ for 12 h. Emission was collected at 500–550 nm for the green channel (excited at 487 nm) and at 550–600 nm for the red channel (excited at 487 nm). Scale bar: 10 μm.

red channel (Figure S8a,b). However, when the cells were loaded with IFN-γ/LPS/L-Arg and further stimulated with compound **B-SH**, the fluorescence dramatically increased (Figure S8c,d). It was reported that NO is able to increase glutathione (GSH) through transcriptional activation of the γ-glutamylsynthetase which catalyzed the rate limiting step in GSH biosynthesis.[40] We speculated that LPS elicits NO in the macrophage as a signature of inflammation, thus, further inducing the augmentation of GSH (regarded as an important antioxidant) to prevent NO intoxication. The results revealed the cross-talk relationship of NO and GSH in the inflammation model, which may provide detailed information in bioapplications such as immunotherapy studies and inflammation relevant drug screening.

In summary, we developed a fluorescence probe **1** for sensing NO and GSH simultaneously for the first time. The probe exhibited significant fluorescence enhancements toward NO and GSH from dual emission channels. Cellular experiments demonstrated that the probe had the capability of monitoring exogenous and endogenous NO and GSH in RAW 264.7 cells. Importantly, probe **1** could visualize the elevation of both NO and GSH in inflammatory mediator induced by IFN-γ/LPS/L-Arg in RAW 264.7 cells, which provided a deeper insight into the physiological relationship of NO and GSH. We expect that this type of fluorescent probe may be promising for better understanding of the physiological roles of NO and GSH.

■ ASSOCIATED CONTENT

Supporting Information

The Supporting Information is available free of charge on the ACS Publications website at DOI: 10.1021/acs.analchem.9b00169.

Materials and apparatus, experimental details, synthesis, and characterization, spectroscopic properties of probes **1**–**3**, cytotoxicity assay, cell imaging, and NMR and HRMS spectra (PDF)

■ AUTHOR INFORMATION

Corresponding Authors

*E-mail: niuly@bnu.edu.cn.
*E-mail: qzyang@bnu.edu.cn.

ORCID

Li-Ya Niu: 0000-0002-5376-6902
Qing-Zheng Yang: 0000-0002-9131-4907

Notes

The authors declare no competing financial interest.

■ ACKNOWLEDGMENTS

We thank Yeguang Fang and Prof. Ganglong Cui for the theoretical calculations. This work was financially supported by National Natural Science Foundation of China (Grants 21525206) and the Fundamental Research Funds for the Central Universities.

■ REFERENCES

(1) Klatt, P.; Lamas, S. *Eur. J. Biochem.* **2000**, *267*, 4928–4944.
(2) Fukumura, D.; Kashiwagi, S.; Jain, R. K. *Nat. Rev. Cancer* **2006**, *6*, 521.
(3) Hausladen, A.; Gow, A. J.; Stamler, J. S. *Proc. Natl. Acad. Sci. U. S. A.* **1998**, *95*, 14100–14105.
(4) Stamler, J. S.; Hausladen, A. *Nat. Struct. Biol.* **1998**, *5*, 247.
(5) Du, J.; Hu, M.; Fan, J.; Peng, X. *Chem. Soc. Rev.* **2012**, *41*, 4511–4535.
(6) Yang, Y.; Zhao, Q.; Feng, W.; Li, F. *Chem. Rev.* **2013**, *113*, 192–270.
(7) Chen, X.; Wang, F.; Hyun, J. Y.; Wei, T.; Qiang, J.; Ren, X.; Shin, I.; Yoon, J. *Chem. Soc. Rev.* **2016**, *45*, 2976–3016.
(8) Mulay, S. V.; Choi, M.; Jang, Y. J.; Kim, Y.; Jon, S.; Churchill, D. G. *Chem. - Eur. J.* **2016**, *22*, 9642–9648.
(9) Sasaki, E.; Kojima, H.; Nishimatsu, H.; Urano, Y.; Kikuchi, K.; Hirata, Y.; Nagano, T. *J. Am. Chem. Soc.* **2005**, *127*, 3684–3685.
(10) Wang, N.; Yu, X.; Zhang, K.; Mirkin, C. A.; Li, J. *J. Am. Chem. Soc.* **2017**, *139*, 12354–12357.
(11) Wang, F.; Yu, S.; Xu, Z.; Li, L.; Dang, Y.; Xu, X.; Luo, Y.; Cheng, Z.; Yu, H.; Zhang, W.; Zhang, A.; Ding, C. *Anal. Chem.* **2018**, *90*, 7953–7962.
(12) Lim, M. H.; Lippard, S. J. *Acc. Chem. Res.* **2007**, *40*, 41–51.
(13) Lim, M. H.; Xu, D.; Lippard, S. J. *Nat. Chem. Biol.* **2006**, *2*, 375.
(14) Mondal, B.; Kumar, P.; Ghosh, P.; Kalita, A. *Chem. Commun.* **2011**, *47*, 2964–2966.
(15) Muthuraj, B.; Deshmukh, R.; Trivedi, V.; Iyer, P. K. *ACS Appl. Mater. Interfaces* **2014**, *6*, 6562–6569.
(16) Reinhardt, C. J.; Zhou, E. Y.; Jorgensen, M. D.; Partipilo, G.; Chan, J. *J. Am. Chem. Soc.* **2018**, *140*, 1011–1018.
(17) Mao, Z.; Jiang, H.; Li, Z.; Zhong, C.; Zhang, W.; Liu, Z. *Chem. Sci.* **2017**, *8*, 4533–4538.
(18) Mao, Z.; Jiang, H.; Song, X.; Hu, W.; Liu, Z. *Anal. Chem.* **2017**, *89*, 9620–9624.
(19) Yuan, L.; Lin, W.; Xie, Y.; Chen, B.; Zhu, S. *J. Am. Chem. Soc.* **2012**, *134*, 1305–1315.
(20) Dai, C.-G.; Wang, J.-L.; Fu, Y.-L.; Zhou, H.-P.; Song, Q.-H. *Anal. Chem.* **2017**, *89*, 10511–10519.
(21) Sun, Y.-Q.; Chen, M.; Liu, J.; Lv, X.; Li, J.-f.; Guo, W. *Chem. Commun.* **2011**, *47*, 11029–11031.
(22) Umezawa, K.; Yoshida, M.; Kamiya, M.; Yamasoba, T.; Urano, Y. *Nat. Chem.* **2017**, *9*, 279.
(23) Kong, F.; Liang, Z.; Luan, D.; Liu, X.; Xu, K.; Tang, B. *Anal. Chem.* **2016**, *88*, 6450–6456.
(24) Xiang, H.; Chen, H.; Tham, H. P.; Phua, S. Z. F.; Liu, J.-G.; Zhao, Y. *ACS Appl. Mater. Interfaces* **2017**, *9*, 27553–27562.
(25) Miao, Q.; Li, Q.; Yuan, Q.; Li, L.; Hai, Z.; Liu, S.; Liang, G. *Anal. Chem.* **2015**, *87*, 3460–3466.
(26) Yin, C.-X.; Xiong, K.-M.; Huo, F.-J.; Salamanca, J. C.; Strongin, R. M. *Angew. Chem., Int. Ed.* **2017**, *56*, 13188–13198.
(27) Niu, L.-Y.; Chen, Y.-Z.; Zheng, H.-R.; Wu, L.-Z.; Tung, C.-H.; Yang, Q.-Z. *Chem. Soc. Rev.* **2015**, *44*, 6143–6160.
(28) Yang, X.-F.; Huang, Q.; Zhong, Y.; Li, Z.; Li, H.; Lowry, M.; Escobedo, J. O.; Strongin, R. M. *Chem. Sci.* **2014**, *5*, 2177–2183.
(29) Mulay, S. V.; Kim, Y.; Choi, M.; Lee, D. Y.; Choi, J.; Lee, Y.; Jon, S.; Churchill, D. G. *Anal. Chem.* **2018**, *90*, 2648–2654.

DOI: 10.1021/acs.analchem.9b00169
Anal. Chem. 2019, 91, 4301–4306

(30) Niu, L.-Y.; Guan, Y.-S.; Chen, Y.-Z.; Wu, L.-Z.; Tung, C.-H.; Yang, Q.-Z. *J. Am. Chem. Soc.* **2012**, *134*, 18928−18931.
(31) Komatsu, H.; Miki, T.; Citterio, D.; Kubota, T.; Shindo, Y.; Kitamura, Y.; Oka, K.; Suzuki, K. *J. Am. Chem. Soc.* **2005**, *127*, 10798−10799.
(32) Kojima, H.; Nakatsubo, N.; Kikuchi, K.; Kawahara, S.; Kirino, Y.; Nagoshi, H.; Hirata, Y.; Nagano, T. *Anal. Chem.* **1998**, *70*, 2446−2453.
(33) Niu, L.-Y.; Guan, Y.-S.; Chen, Y.-Z.; Wu, L.-Z.; Tung, C.-H.; Yang, Q.-Z. *Chem. Commun.* **2013**, *49*, 1294−1296.
(34) Liu, X.-L.; Niu, L.-Y.; Chen, Y.-Z.; Yang, Y.; Yang, Q.-Z. *Biosens. Bioelectron.* **2017**, *90*, 403−409.
(35) Zhang, X.; Wu, Y.; Ji, S.; Guo, H.; Song, P.; Han, K.; Wu, W.; Wu, W.; James, T. D.; Zhao, J. *J. Org. Chem.* **2010**, *75*, 2578−2588.
(36) Kojima, H.; Urano, Y.; Kikuchi, K.; Higuchi, T.; Hirata, Y.; Nagano, T. *Angew. Chem., Int. Ed.* **1999**, *38*, 3209−3212.
(37) Lee, H. Y.; Choi, Y. P.; Kim, S.; Yoon, T.; Guo, Z.; Lee, S.; Swamy, K. M. K.; Kim, G.; Lee, J. Y.; Shin, I.; Yoon, J. *Chem. Commun.* **2014**, *50*, 6967−6969.
(38) McQuade, L. E.; Ma, J.; Lowe, G.; Ghatpande, A.; Gelperin, A.; Lippard, S. J. *Proc. Natl. Acad. Sci. U. S. A.* **2010**, *107*, 8525−8530.
(39) Winyard, P. G.; Ryan, B.; Eggleton, P.; Nissim, A.; Taylor, E.; Lo Faro, M. L.; Burkholz, T.; Szabó-Taylor; Katalin, E.; Fox, B.; Viner, N.; Haigh, R. C.; Benjamin, N.; Jones, A. M.; Whiteman, M. *Biochem. Soc. Trans.* **2011**, *39*, 1226−1232.
(40) Eiserich, J. P.; Patel, R. P.; O'Donnell, V. B. *Mol. Aspects Med.* **1998**, *19*, 221−357.

DOI: 10.1021/acs.analchem.9b00169
Anal. Chem. 2019, 91, 4301−4306